Chapter3
Optically pumped GaN-based VCSEL

3.1 Recent Status

GaN based materials have been attracting a great deal of attention due to the large direct band gap and the promising potential for the optoelectronic devices, including light emitting diodes(LEDs) and laser diodes(LDs). Recently, many efforts were devoted to the development of GaN-based vertical-cavity surface emitting laser (VCSEL). The VCSEL possesses many advantageous properties over the edge emitting laser, including circular beam shape, light emission in vertical direction, and formation of two-dimensional arrays. In particular, the use of two-dimensional arrays of the blue VCSELs could reduce the read-out time in high density optical storage and increase the scan speed in high-resolution laser printing technology [39]. The realization of the VCSEL requires a pair of high-reflectivity mirrors, usually in the form of DBRs, for forming a high-Q vertical cavity. Two types of the epitaxially grown high-reflectivity nitride mirrors were reported earlier using GaN/$Al_xGa_{1-x}N$ DBR with different aluminum content. Someya et al. [8] used 43 pairs of $Al_{0.34}Ga_{0.66}N$/GaN as the bottom DBR and reported the lasing action at ~400nm. Zhou et al [11] employed a bottom DBR of 60 pairs $Al_{0.25}Ga_{0.75}N$/GaN and observed the lasing action at 383.2nm. All these AlGaN/GaN DBR structures required large numbers of pairs due to the relatively low refractive index contrast between $Al_xGa_{1-x}N$ and GaN. The DBR structure using AlN/GaN has higher refractive index contrast ($\Delta n/n=0.16$) [40] that can achieve high reflectivity with relatively less numbers of pairs. It also has wide stop band that can easily align with the active layer emission peak to achieve lasing action. Therefore, the AlN/GaN is attractive for application in nitride VCSEL. However, the AlN/GaN combination has relatively large lattice mismatch (~2.4%) and the difference in thermal expansion coefficients between GaN (5.59×10^{-6}/K) and AlN (4.2×10^{-6}/K) that tends to cause cracks in the epitaxial film during the growth of the AlN/GaN DBR structure and could result in the reduction of reflectivity and increase in scattering loss. Recently, we have achieved high-reflectivity AlN/GaN DBR structure with a peak reflectance of 94% and a stop band about 18nm with relatively smooth surface morphology [23]. Such AlN/GaN DBR with high reflectivity incorporated in the GaN vertical cavity light emitting device has shown to enhance the light emission intensity due to the resonant cavity effect [24].

In this section, we report the design and fabrication of GaN-based VCSEL using the AlN/GaN DBRs as the bottom mirror and a Ta_2O_5/SiO_2 dielectric multiple layer structure as the top DBR mirror, and demonstration of the laser operation under optical pumping at room temperature.

3.2 The Design of GaN-based VCSEL [41-43]

Typical VCSEL structure is composed of two dominant components: the center active region provides gain, and a pair of high-reflectivity DBRs which form a high quality Fabry-Perot resonant cavity. Therefore, the design of active region and the choice of DBRs are quite important. A favorite design of GaN-based VCSEL is the hybrid structure employed the in-situ epitaxial grown semiconductor DBR, and the dielectric DBR. Compared to the structure with all epitaxial grown DBRs or all dielectric DBRs, the hybrid one is more easy and convenient. Here, the simulation of useful design of GaN-based VCSEL with hybrid structure and active region located at the area of strong electric field intensity in the resonant cavity were reported. The design is simulated by the thin film design software TFCalc published by Software Spectra Inc of Portland, OR, USA.

3.2.1 The Simulation of Ta_2O_5/SiO_2 and Nitride-based DBRs

The simulation of nitride-based DBRs [44]

The nitride-based DBR is currently major candidate for fabrication of nitride-based VCSEL. In general, the choices of the nitride-based DBR are the combinations of $Al_xGa_{1-x}N$/GaN DBRs. We simulated and discussed the reflectance of three $Al_xGa_{1-x}N$/GaN DBRs:$Al_{0.25}Ga_{0.75}N$/GaN DBRs, $Al_{0.35}Ga_{0.65}N$/GaN DBRs, and AlN/GaN DBRs, to understand the performance of these DBRs. The incident angle of illumination and wavelength of the reference light used in the simulation were 0^o and 450nm, respectively.

(Ⅰ)$Al_{0.25}Ga_{0.75}N$/GaN DBRs

The refractive index of GaN and $Al_{0.25}Ga_{0.75}N$ at wavelength of 450nm, used as the parameters in the simulation, were n_{GaN} = 2.45 and $n_{Al0.25Ga0.75N}$ = 2.35. Figure 3.1 shows the reflectance spectrum of 25, 40, 60, and 80 pairs of $Al_{0.25}Ga_{0.75}N$/GaN DBR. The $Al_{0.25}Ga_{0.75}N$/GaN mirror with 80 pairs of DBR can achieve the high reflectivity of 98% and the FWHM of reflectance spectrum about 13nm

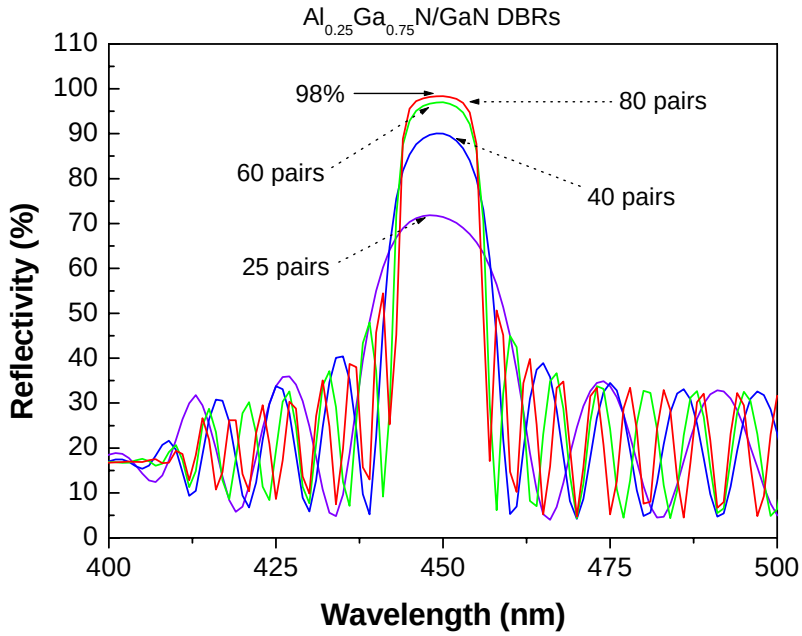

Figure 3.1 The reflectance spectrum of 25, 40, 60, and 80 pairs of $Al_{0.25}Ga_{0.75}N$/GaN DBR

(Ⅱ)$Al_{0.35}Ga_{0.65}N$/GaN DBRs

The refractive index of GaN and $Al_{0.35}Ga_{0.65}N$ at wavelength of 450nm, used as the parameters in the simulation, were n_{GaN} = 2.45 and $n_{Al0.35Ga0.65N}$ = 2.31. Figure 3.2 shows the reflectance spectrum of 25, 30, 40, and 50 pairs of $Al_{0.35}Ga_{0.65}N$/GaN DBR. The $Al_{0.35}Ga_{0.65}N$/GaN mirror with 50 pairs of DBR can achieve the high reflectivity of 98% and the FWHM of reflectance spectrum about 19nm.

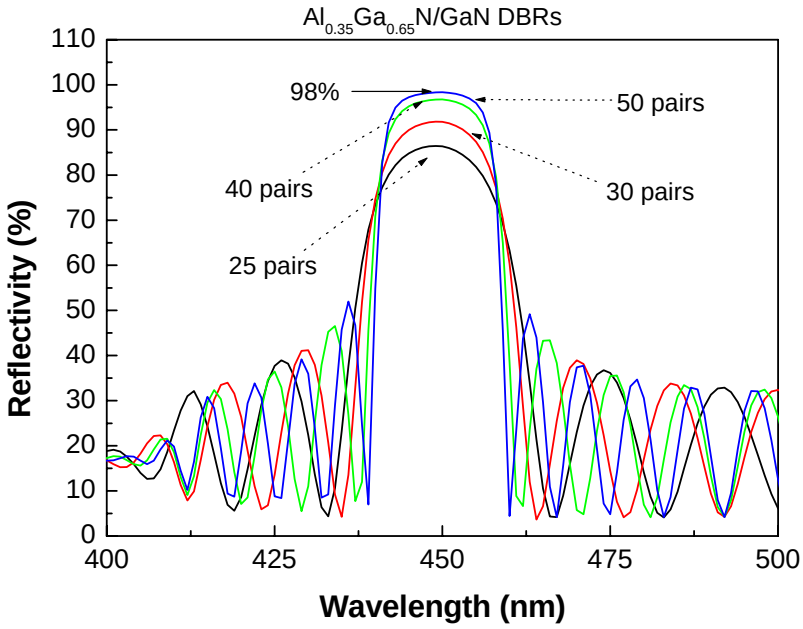

Figure 3.2 The reflectance spectrum of 25, 30, 40, and 50 pairs of $Al_{0.35}Ga_{0.65}N$/GaN

(Ⅲ)AlN/GaN DBRs

The refractive index of GaN and AlN at wavelength of 450nm, used as the fundamental parameters in the simulation, were n_{GaN} = 2.45 and n_{AlN} = 2.10. Figure 3.3 shows the reflectance spectrum of 5, 10, 15, and 25 pairs of AlN/GaN DBR. The AlN/GaN mirror with 25 pairs of DBR can achieve the high reflectivity of 99% and the wide FWHM of reflectance spectrum about 46nm.

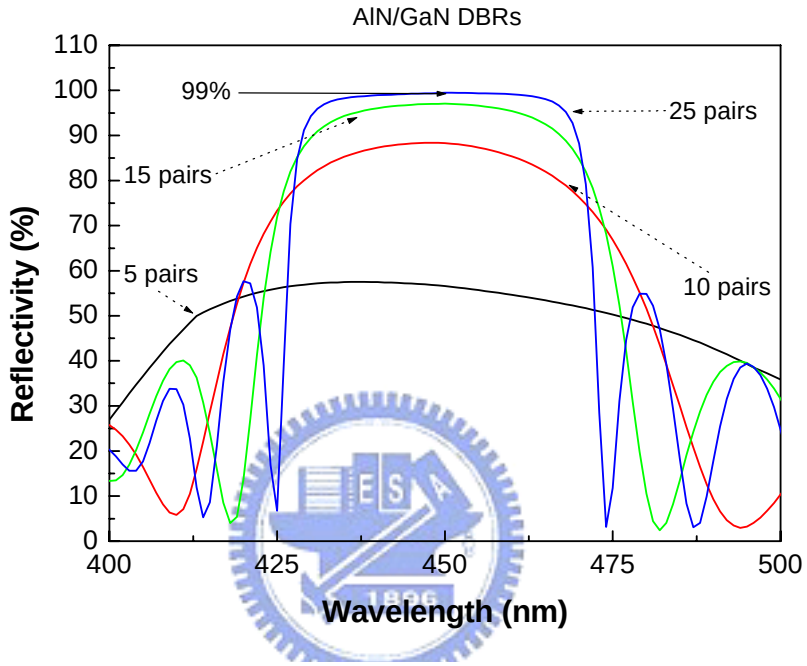

Figure 3.3 The reflectance spectrum of 5, 10, 15, and 25 pairs of AlN/GaN DBR.

(Ⅳ)Comparison of nitride-based DBRs

In this part, we compare the three different nitride-based DBRs mentioned before. Figure 3.4 shows the reflectance spectrum of three different nitride-based DBRs with high reflectivity. From all the previous simulation results, it is obviously that the high Al content $Al_xGa_{1-x}N$/GaN mirrors have less pairs of DBR needed to form high reflectivity mirror with wide FWHM of reflectance spectrum. Therefore, AlN/GaN-based DBRs should be the best choice to be employed as the bottom mirror of GaN-based VCSEL. In this study, we used 25 pairs of AlN/GaN DBR as the bottom mirror.

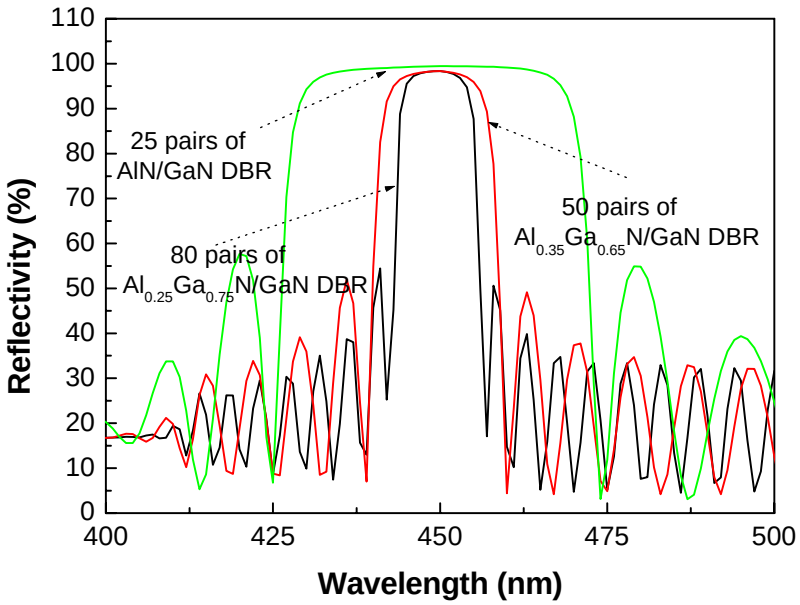

Figure 3.4 The reflectance spectrum of three different nitride-based DBRs with high reflectivity.

The simulation of Ta_2O_5/SiO_2 DBRs [30] [45]

Dielectric DBR mirror has the advantage of the large refractive index contrast between two different dielectric materials that it only needs fewer pairs of DBR to form high reflectivity mirror. In most dielectric DBRs, the SiO_2 is usually used as the low refractive index material due to its relative low refractive index than many other dielectric materials and some advantaged characteristics. It is easy and cheap to get, hard to decompose, and high transparent form the wavelength of 180nm to 8μm. As to the high refractive index material, the Ta_2O_5 with benefits of low absorption and high transparency in visible to IR ray is a proper selection. The refractive index of SiO_2 and Ta_2O_5 at wavelength of 450nm, used as the fundamental parameters in the simulation, are $n_{SiO2} = 1.463$ and $n_{Ta2O5} = 2.15$. Figure 3.5 shows the reflectance spectrum of 3, 5, and 8 pairs of Ta_2O_5/SiO_2 DBR. The Ta_2O_5/SiO_2 mirror with 8 pairs of DBR can achieve the high reflectivity of 99% and the wide FWHM of reflectance spectrum about 128nm. Therefore, we chose 8 pairs of Ta_2O_5/SiO_2 DBR as the top mirror in the following experiments.

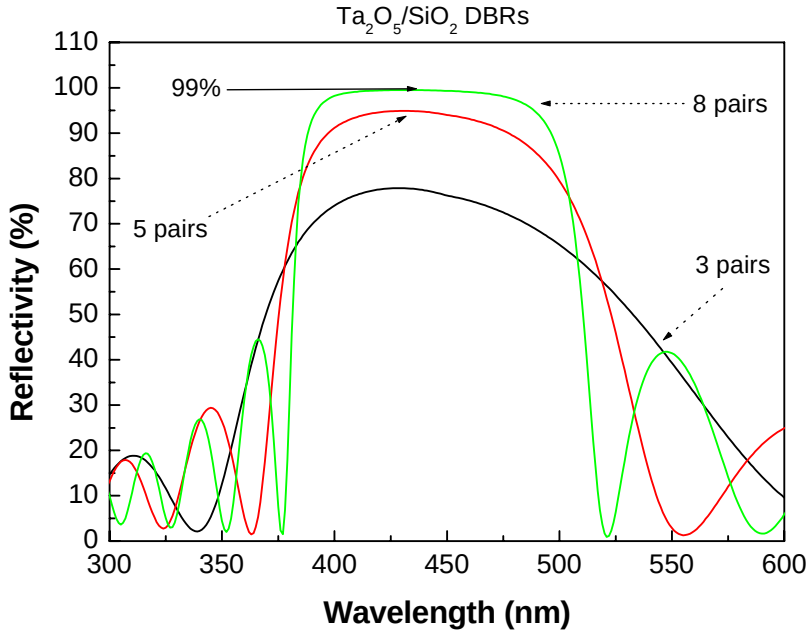

Figure 3.5 The reflectance spectrum of 3, 5, and 8 pairs of Ta_2O_5/SiO_2 DBR.

3.2.2 The Design of Active Region

In addition to the consideration of high-reflectivity mirror, the design of active region, usually in the form of MQW, is also an important issue to the fabrication of GaN-based VCSEL. In our design, the optical thickness (OT) is threeλ_0 (about 1350nm), and the relative geometrical thickness is about threeλ_0 over refractive index n_0 ($3\lambda_0/n_0$). The active region plays the role of the gain medium of VCSEL, and the number of InGaN/GaN MQW determines the gain. It seems like that the more MQWs employed, the more gain can be got. In fact, too many pairs of MQW will lower the value of the gain due to the re-absorption exists in MQW. We employ ten pairs of MQW, composed of 3nm $In_{0.2}Ga_{0.8}N$ and 7nm GaN, into the active region. The thickness of p-GaN and n-GaN were determined as 100nm and 380nm, respectively. Finally, the electrical field intensity (EFI) of a well designed structure including active region and both reflecting mirror was simulated. Figure 3.6 shows the EFI and the refractive index relative as the functions of the distance from top layer. It can be observed that a pronounced resonant enhancement of the electric field was built up in the active region. It suggests that the light could be amplified inside the resonant cavity and the more opportunity could be obtained to achieve laser operation.

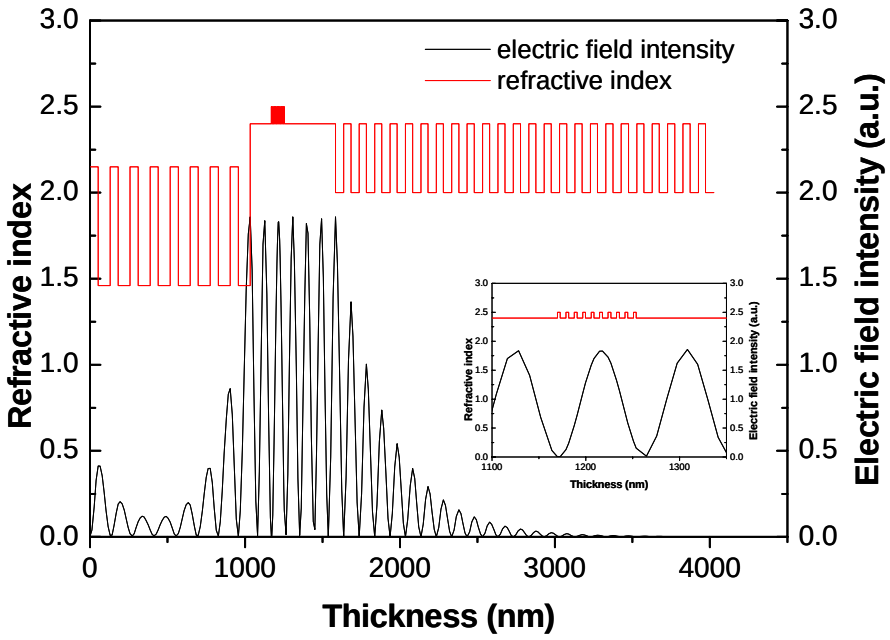

Figure 3.6 The EFI and the refractive index relative as the functions of the distance from top layer.

3.3 The Fabricated GaN-based VCSEL Structure

3.3.1 Fabrication of GaN-based VCSEL

The structure of the GaN-based VCSEL was grown in a vertical-type MOCVD system (EMCORE D-75) with a fast rotating disk, which can hold one 2-inch wafer. The polished optical-grade C-face (0001) 2-inch-diameter sapphire was used as substrate for the epitaxial growth of the VCSEL structure. Trimethylindium (TMIn), Trimethylgallium (TMGa), Trimethylaluminum (TMAl), and ammonia (NH_3) were used as the In, Ga, Al, and N sources, respectively. Initially, a thermal cleaning process was carried out at 1080°C for 10 minutes in a stream of hydrogen ambient before the growth of epitaxial layers. After depositing a 30-nm-thick GaN nucleation layer at 530°C, the temperature was raised up to 1045°C for the growth of a 1-μm-thick GaN buffer layer. Then a 25-pairs AlN/GaN DBR structure was grown at 1040°C under the fixed chamber pressure of 100 Torr similar to the previous reported growth condition [23-24]. Then a 380-nm-thick n-type GaN, followed by a ten pairs $In_{0.2}Ga_{0.8}N$ MQW and a 100-nm-thick p-type GaN were grown to form a 3 λ cavity. Finally, an eight pairs Ta_2O_5/SiO_2 dielectric mirror was deposited by the E-gun as the top DBR reflector. The SEM image of the MOCVD grown structure and the overall VCSEL structure are shown in the Fig 3.7(a) and (b). The schematic diagram of the overall VCSEL structure is shown in Fig. 3.7(c).

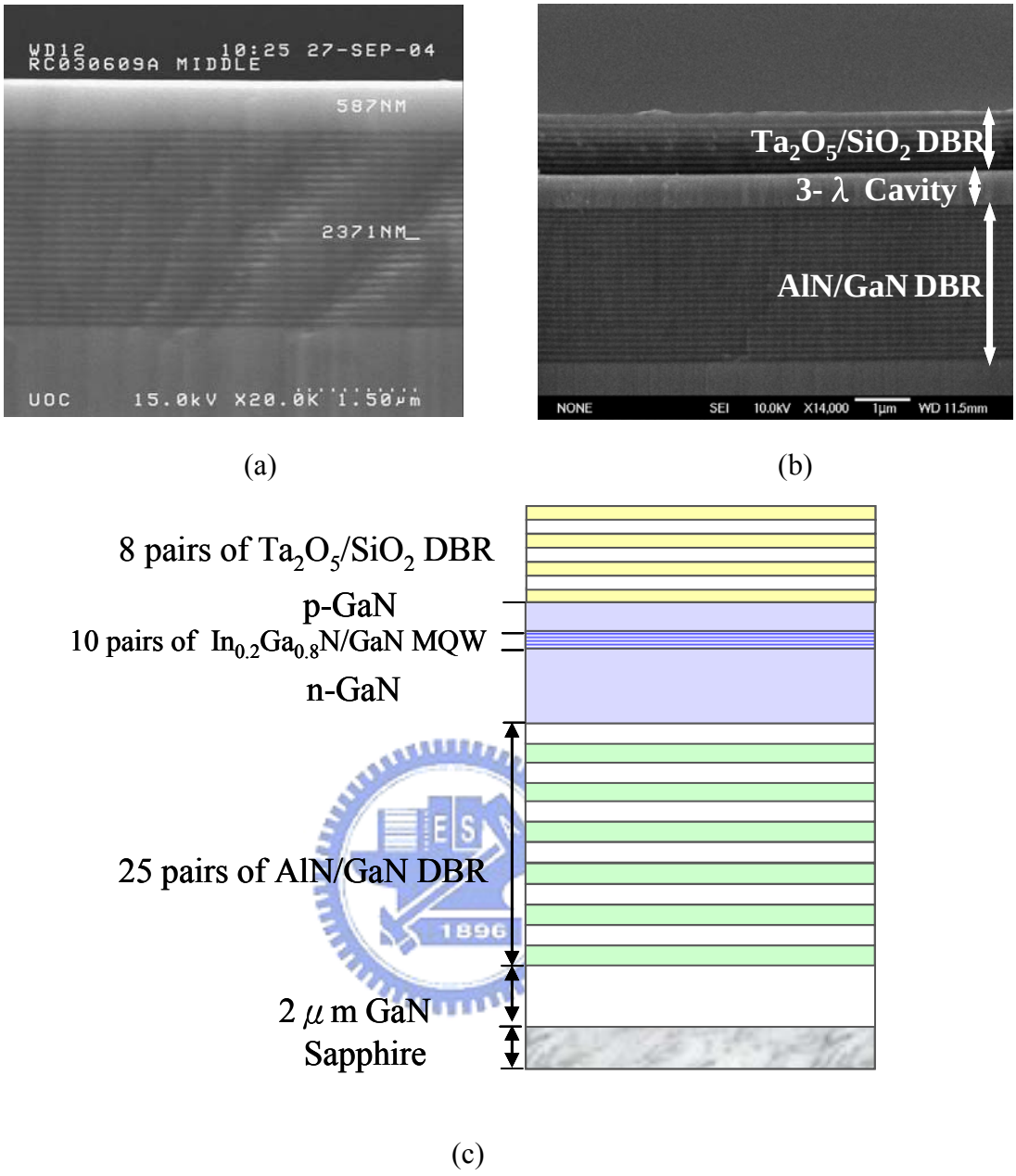

Figure 3.7(a) The SEM image of the MOCVD grown structure (b) The SEM image of the overall VCSEL (c) The schematic diagram of the overall VCSEL structure

3.3.2 Reflectance Spectrum and Photoluminescence

Reflectance spectrum

The structure of GaN-based VCSEL is fabricated as discussed previously. The reflectance spectrum of the 25 pairs of AlN/GaN DBR grown on the sapphire by the MOCVD and the 8 pairs of Ta_2O_5/SiO_2 DBR evaporated on the Si substrate by E-gun were measured by the n&k ultraviolet-visible spectrometer with normal incidence at room temperature. Figure 3.8 shows the reflectance spectrum of AlN/GaN DBRs and Ta_2O_5/SiO_2 DBRs, respectively. The AlN/GaN mirror with 25 pairs of DBR can achieve the high reflectivity of 94% and the

wide FWHM of reflectance spectrum about 33nm. The Ta_2O_5/SiO_2 mirror with 8 pairs of DBR can achieve the high reflectivity of 97.5% and the wide FWHM of reflectance spectrum about 115nm.

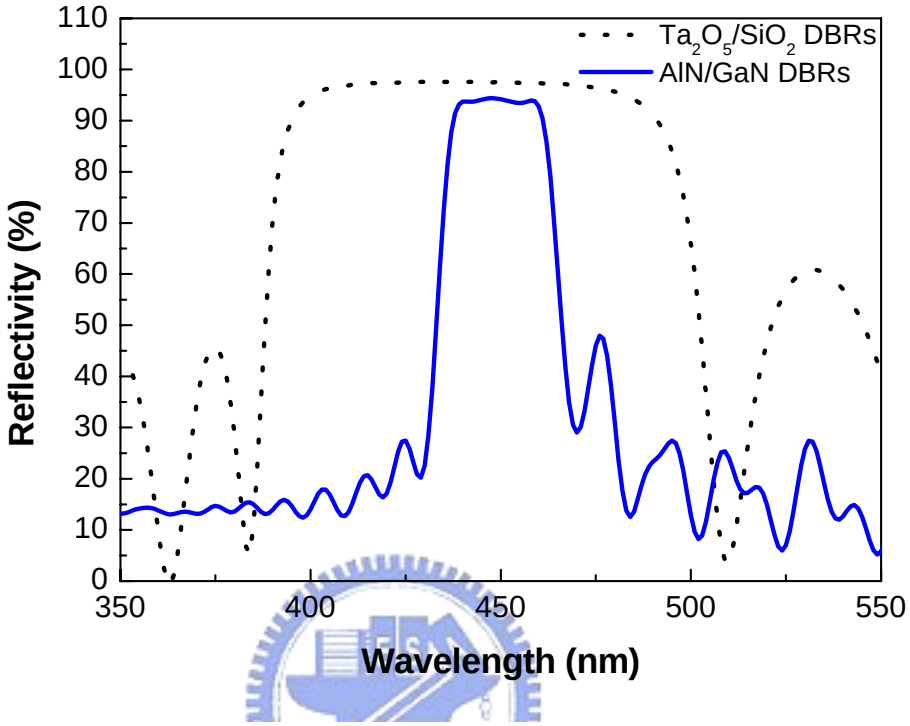

Figure 3.8 The reflectance spectrum of AlN/GaN DBRs and Ta_2O_5/SiO_2 DBRs.

Photoluminescence

The photoluminescence (PL) emission was excited by a 325nm He-Cd laser with a spot size of about 2-μm-diameter. By using the microscopy system (WITec, alpha snom), the emission was collected into a spectrometer/CCD (Jobin-Yvon Triax 320 Spectrometer) with a spectral resolution of ~0.1nm for spectral output measurement. Figure 3.9 shows the PL emission of the MOCVD grown structure and overall VCSEL structure. The PL emission peak wavelength and the FWHM of emission spectrum of MOCVD grown structure were 448nm and 10.5nm, respectively. It is obviously that the PL emission peak wavelength of overall VCSEL structure was dominated by cavity mode and was centered at 448nm. The PL emission of and the FWHM of emission spectrum of overall VCSEL structure were 448nm and 1.4nm, respectively. The narrow FWHM of 1.4nm is attributed to the Febry-Perot cavity effect.

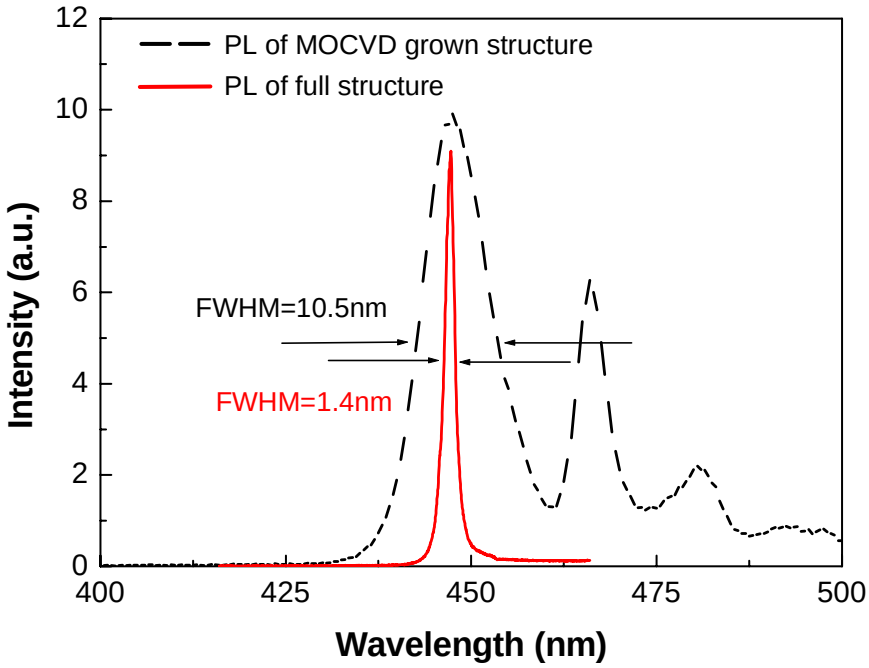

Figure 3.9 PL emission of MOCVD grown structure and overall VCSEL structure.

3.3.3 The Finesse and the Quality Factor

A narrow PL emission with full width at half maximum of 1.4nm corresponds to the cavity resonant mode at 448nm was observed. It indicates the emission peak was well-aligned with vertical cavity formed by the high reflectance of AlN/GaN DBR and the Ta_2O_5/SiO_2 dielectric mirror. The cavity finesse and the cavity quality factor are defined as $F = \frac{\Delta\phi}{\delta\phi} = \frac{\pi}{2\phi_{1/2}} = \frac{\pi}{1-\sqrt{R_1R_2}}$ and $Q = \frac{\phi}{\delta\phi} = \frac{2nL_c}{\lambda}\frac{\pi}{1-\sqrt{R_1R_2}}$. The cavity finesse and the cavity quality factor, estimated from the emission linewidth of 1.4nm, are about 53 and 320. These values agree with the theoretical calculation while the absorption loss is considered.

3.4 Optical Pumping Experiment

3.4.1 Optical Pumping System

The optical pumping of the sample was performed using a frequency-tripled Nd:YVO_4 355-nm pulsed laser with a pulse width of ~ 0.5 ns at a repetition rate of 1 kHz. The pumping laser beam with a spot size of 60 μm was incident normal to the VCSEL sample surface. By using the microscopy system (WITec, alpha snom), the light emission from the VCSEL sample was collected into a spectrometer/CCD (Jobin-Yvon Triax 320 Spectrometer) with a spectral resolution of ~0.1nm for spectral output measurement. Figure 3.10 shows the schematic of optical pumping system.

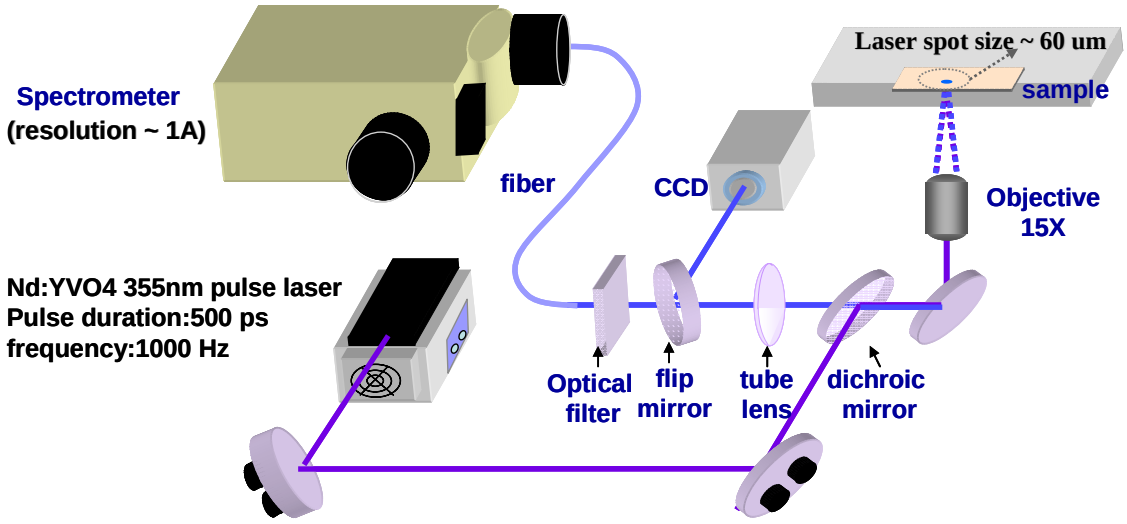

Figure 3.10 Optical pumping system.

3.4.2 The Characteristics of Optically Pumped GaN-based VCSEL

In this part, we present the characteristics of optically pumped GaN-based VCSEL such as excitation energy - emission intensity curve (L-I), near field pattern (NFP), far field pattern (FFP), threshold carrier density (N_{th}), threshold gain(g_{th}), degree of polarization (DOP), temperature dependent threshold and characteristic temperature (T_0). Through these complete discussions, the performance of the VCSEL could be well realized.

Stimulated emission (lasing)

The stimulated emission of fabricated GaN-based VCSEL was achieved and observed by using the optical pumping system mentioned before. The light emission intensity from the VCSEL as a function of the exciting energy is shown in the Fig 4.11. A distinct threshold characteristic was observed at the threshold pumping energy (E_{th}) of about 1.5μJ corresponding to an energy density of 53mJ/cm^2. Then the laser output increased linearly with the excitation energy beyond the threshold. The inset of the Fig 3.11 shows the excitation energy dependent emission spectrum. It evidently expresses the behavior form spontaneous emission to stimulated emission.

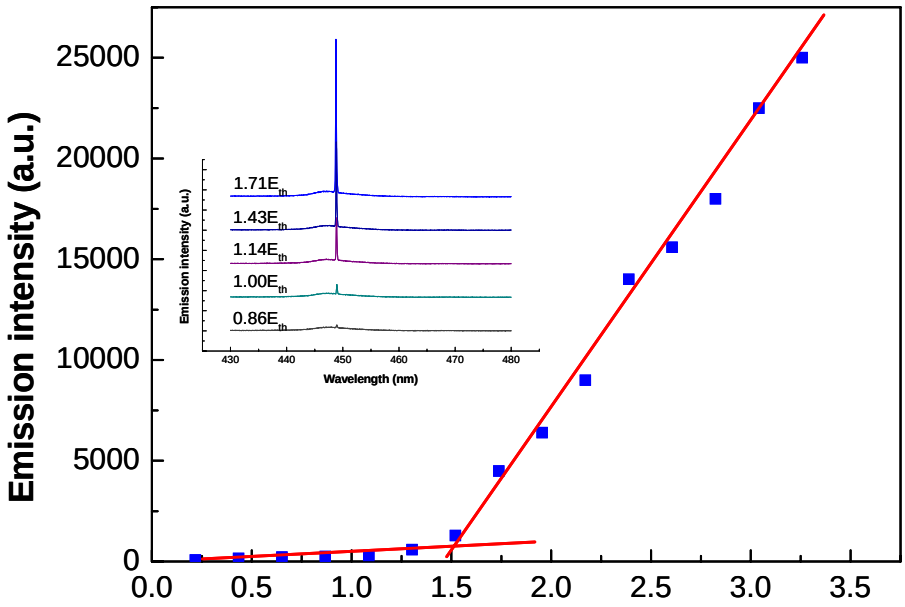

Figure 3.11 The excitation energy - emission intensity curve (L-I).

Figure 3.12 shows the stimulated emission spectrum of the VCSEL at room temperature and the inset shows the stimulated emission image of the VCSEL at 1.17Eth. The laser spot size is estimated about 3μm. The emission peak wavelength and FWHM of the stimulated emission spectrum were about 448nm and 0.17nm.

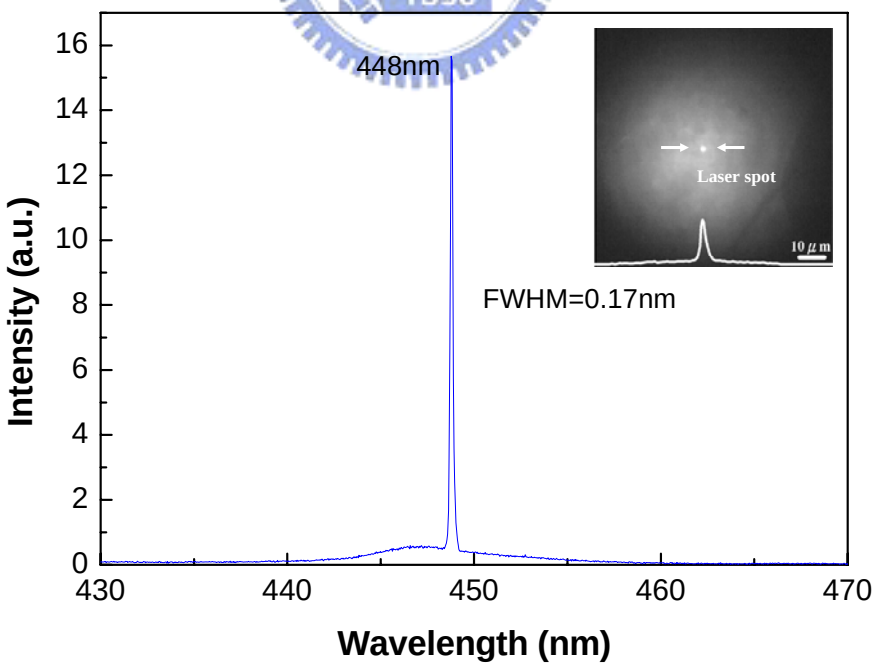

Figure 3.12 The stimulated emission spectrum of the VCSEL at room temperature and the inset shows the stimulated emission image.

The excitation power dependent emission spectrum is a good evidence to prove the occurrence of the stimulated emission. Figure 3.13(a) shows the spontaneous emission image at $0.86E_{th}$ and Fig. 3.13(b) shows appearance of the stimulated emission at $1.00E_{th}$. The stimulated emission spot appears as the excitation energy increased above the threshold excitation energy and shows a bright spot at $1.71E_{th}$. Figure 3.13(c)(d) show the emission image at $1.14E_{th}$, and $1.71E_{th,}$ respectively.

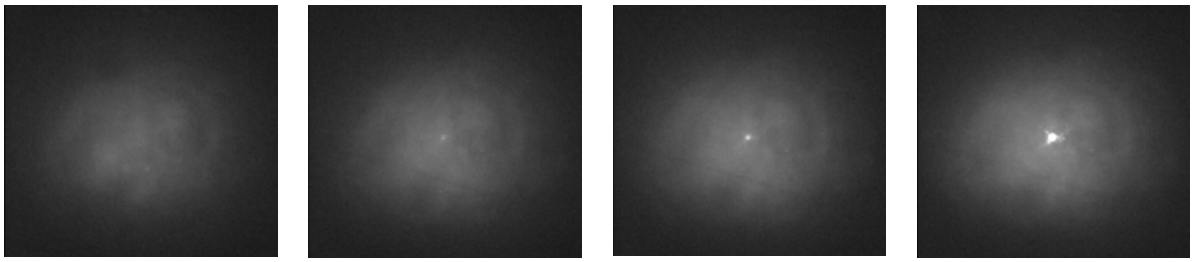

(a)$0.86E_{th}$ (b)$1.00E_{th}$ (c)$1.14E_{th,}$ (d)$1.71E_{th,}$

Figure 3.13 The stimulated emission image at different excitation energy.

Threshold gain and carrier density

An estimation of the carrier density at the threshold was about 3×10^{20} cm^{-3}, assuming the reflectivity of the top mirror at pumping wavelength of 355nm was 40%, the absorption coefficient of the GaN was about 10^5 cm^{-1} at 355nm [46]and the quantum efficiency was 10%. We estimated the threshold gain (g_{th}) of our VCSEL cavity using the equation $g_{th} \cong (1/2N_wL_w)\ln(1/R_1R_2)$, where N_w is the number of quantum wells, L_w is the width of each quantum well and R_1, R_2 are the reflectivity of the top and bottom mirrors, respectively. We obtained the required threshold gain is about 1.45×10^4 cm^{-1} which is roughly in agreement with the gain value estimated based on the Nakamura's report [47]of the gain coefficient of InGaN at our threshold carrier density and slightly higher than the gain value of Park's report[48].

Near field pattern (NFP) and far field pattern (FFP)

The near field pattern (NFP) and far field pattern (FFP) of the stimulated emission were detected by the CCD, analyzed by the Beam View Analyzer software, and discussed along the x-axis and y-axis across the emission center, as shown in Fig 3.14 and Fig. 3.15. Figure 3.14 shows the stimulated emission intensity as a function of the distance from the center of the emission spot. The beam width of FWHM and $1/e^2$ were about 1.3μm and 3.0μm, respectively. Figure 3.15 shows the stimulated emission intensity as a function of the angle along the optical axial of the stimulated emission. The divergence angle of FWHM and $1/e^2$ were about

7.6° and 11.2°, respectively. To both NFP and FFP, it was evident that the intensity distributions along both axes are almost the same, either the peak intensity or the Gaussian distributed intensity. It also clearly proved that the shape of the laser emission is close to circle.

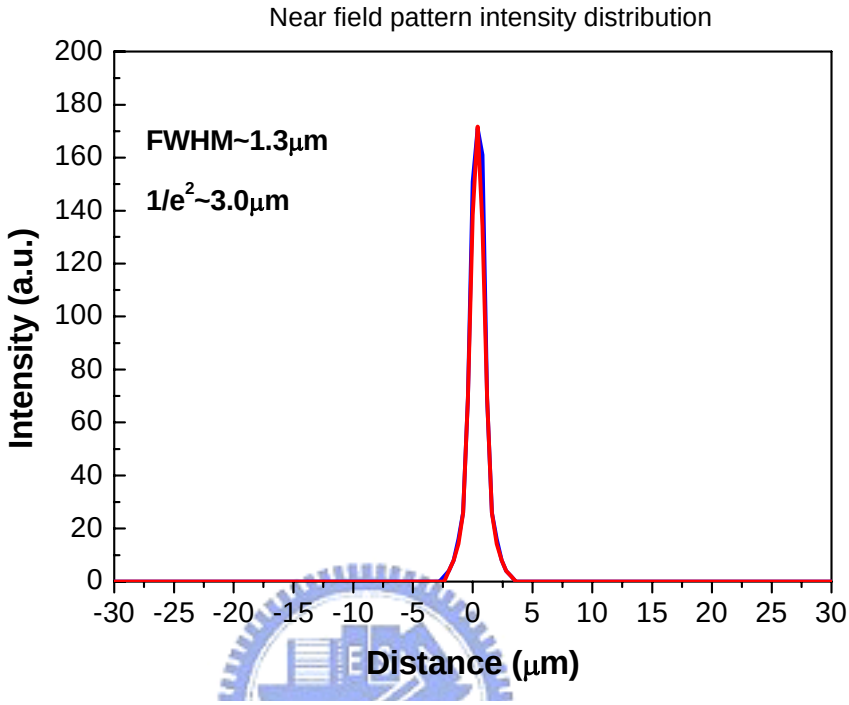

Figure 3.14 The stimulated emission intensity as a function of the distance from the center of the emission spot.

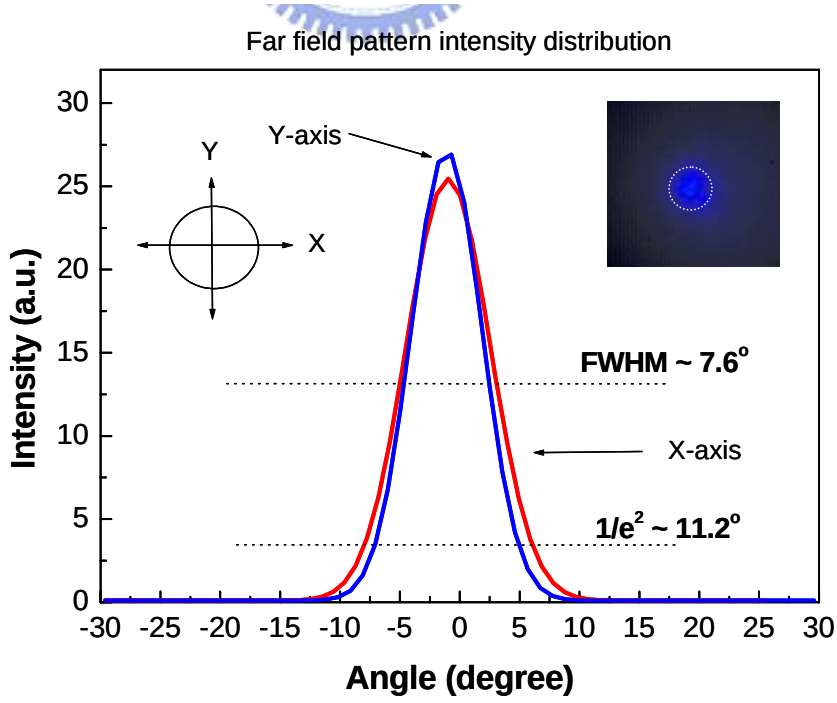

Figure 3.15 The stimulated emission intensity as a function of the angle along the optical axial of the stimulated emission.

Degree of polarization (DOP)

The degree of polarization (DOP) expresses the polarized property of the laser emission. It is defined as DOP= $(I_{max}-I_{min}) / (I_{max}-I_{min})$. Figure 4.16 shows the normalized intensity as a function of the angle of the polarizer. It is nearly a cosine square function. The contrast of laser emission intensity between two orthogonal polarizations was measured. The result showed the laser beam has a degree of polarization of about 84% suggesting strong polarization property of the laser emission.

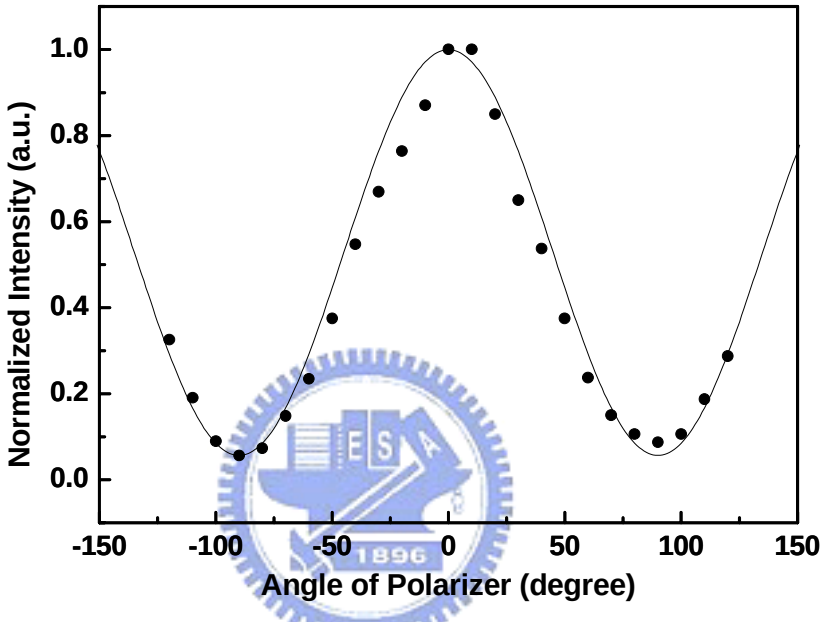

Figure 3.16 The normalized intensity as a function of the angle of the polarizer.

Temperature dependent threshold and characteristic temperature

Besides the basic characteristics of fabricated GaN-based VCSEL at room temperature, we also investigated the behavior of the VCSEL at low temperature. The temperature was lowered by using the liquid nitrogen and controlled by the thermo controller. Figure 3.17 shows the temperature dependent threshold excitation energy. The solid line in Fig 3.17 represents the best fit of the experimental data to the empirical form $I_{th(T)}=I_o\exp(T/T_o)$, where I_{th} is the threshold excitation energy, I_0 is a constant, T is the absolute temperature in degrees Kelvin, K, and T_0 is the characteristic temperature. Characteristic temperature T_0 is an indicator of the laser sensitivity to temperature. High T_0 indicates good temperature tolerance. The characteristic temperature T_o, was estimated to be 243K in the temperature range of 120-300K. The emission intensity-excitation power curve at 120K, 200K, and 300K are

shown in Fig 3.18. It was observed that the increase in temperature leads to an increase in threshold excitation energy. It is due to the increase of non-radiated recombination and decrease of radiated recombination. In other words, the internal quantum efficiency is decreased. The gain depends on the radiated recombination. Therefore, the higher temperature decreases gain and leads to an increase in stimulated emission threshold.

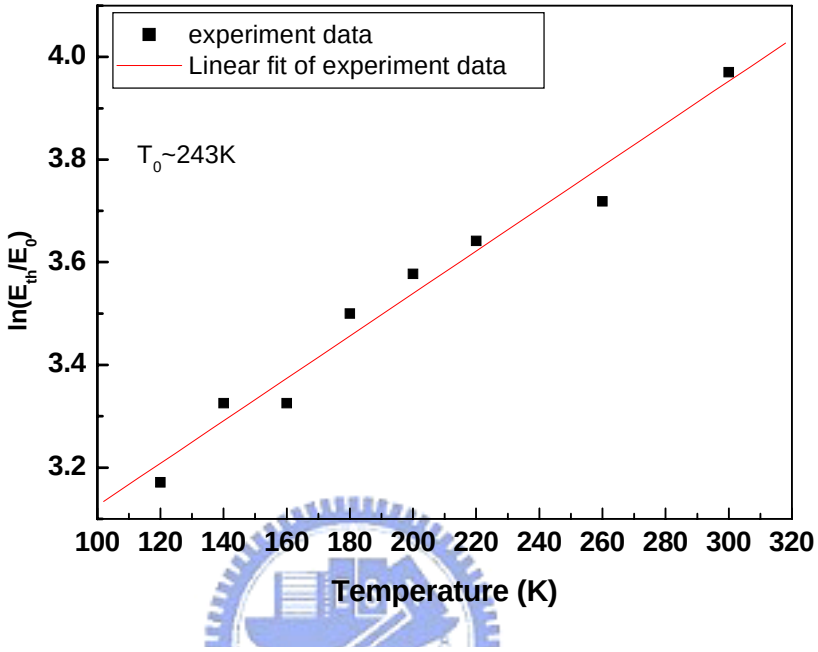

Figure 3.17 The temperature dependent threshold excitation power.

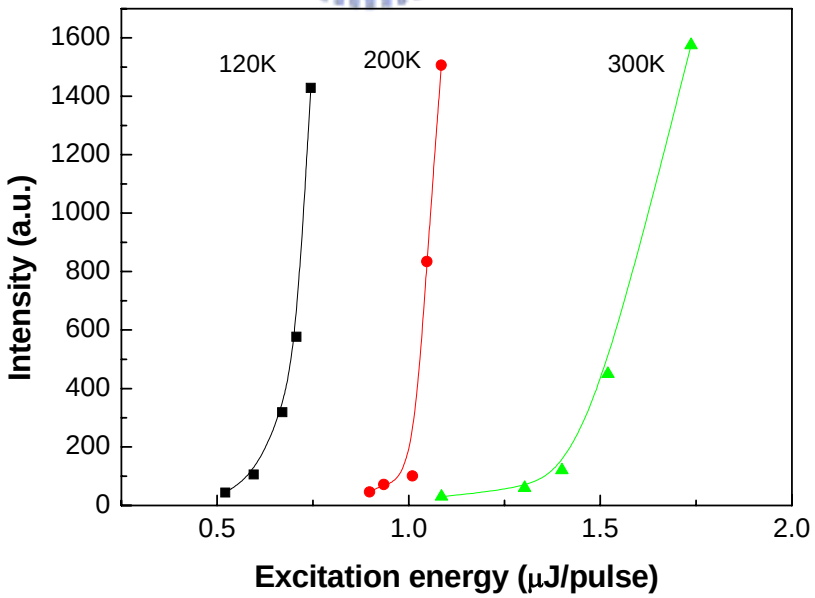

Figure 3.18 The emission intensity-excitation energy curve at 120K, 200K, and 300K.

3.4 Summary

In conclusion, a GaN-based VCSEL with hybrid DBR mirrors, consisting of 25 pairs of AlN/GaN DBR (with reflectivity about 94%) and 8 pairs of Ta_2O_5/SiO_2 DBR (with reflectivity about 97.5%), was fabricated. A narrow PL emission with full width at half maximum of 1.4nm corresponds to the cavity resonant mode at 448nm was observed. The cavity finesse and the cavity quality factor, estimated from the emission linewidth of 1.4nm, are about 53 and 320. The laser action was achieved under the optical pumping at room temperature with a threshold pumping energy density of about 53mJ/cm^2. The GaN VCSEL emits 448nm blue wavelength with a linewidth of 0.17nm. The estimation of the carrier density and gain at the threshold were about 3×10^{20} cm^{-3} and 1.45×10^{4} cm^{-1}, respectively. The NFP and FFP showed that the beam width and divergence angle were about 3.0μm and 7.6^{o}, respectively. The NFP and FFP also indicated that the shape of laser emission was close to a circle. The laser beam showed a degree of polarization of about 84% suggesting strong polarization property of the laser emission. The characteristic temperature of fabricated VCSEL was about 243K suggesting good temperature tolerance.